AGU PUBLICATIONS

JGR

Journal of Geophysical Research: Space Physics

RESEARCH ARTICLE

10.1002/2015JA021327

Key Points:
- Simultaneous EMIC and chorus wave occurrence in the Earth's outer magnetosphere
- High pitch angle transport rate of relativistic electrons by coherent EMIC waves
- EMIC waves more efficient than chorus for relativistic electron pitch angle loss

Correspondence to:
B. Remya,
remyaphysics@gmail.com

Citation:
Remya, B., B. T. Tsurutani, R. V. Reddy, G. S. Lakhina, and R. Hajra (2015), Electromagnetic cyclotron waves in the dayside subsolar outer magnetosphere generated by enhanced solar wind pressure: EMIC wave coherency, *J. Geophys. Res. Space Physics*, *120*, 7536–7551, doi:10.1002/2015JA021327.

Received 17 APR 2015
Accepted 21 AUG 2015
Accepted article online 27 AUG 2015
Published online 26 SEP 2015
Corrected 23 NOV 2015

This article was corrected on 23 NOV 2015. See the end of the full text for details.

©2015. American Geophysical Union. All Rights Reserved.

Electromagnetic cyclotron waves in the dayside subsolar outer magnetosphere generated by enhanced solar wind pressure: EMIC wave coherency

B. Remya[1,2], B. T. Tsurutani[3], R. V. Reddy[1], G. S. Lakhina[1], and R. Hajra[4]

[1]Indian Institute of Geomagnetism, Navi Mumbai, India, [2]Institute of Earth Sciences, Academia Sinica, Taipei, Taiwan, [3]Jet Propulsion Laboratory, California Institute of Technology, Pasadena, California, USA, [4]Instituto Nacional de Pesquisas Espaciais, Sao Jose dos Campos, Brazil

Abstract Electromagnetic ion (proton) cyclotron (EMIC) waves and whistler mode chorus are simultaneously detected in the Earth's dayside subsolar outer magnetosphere. The observations were made near the magnetic equator 3.1°–1.5° magnetic latitude at 1300 magnetic local time from $L = 9.9$ to 7.0. It is hypothesized that the solar wind external pressure caused preexisting energetic 10–100 keV protons and electrons to be energized in the $T_\perp$ component by betatron acceleration and the resultant temperature anisotropy ($T_\perp > T_\parallel$) formed led to the simultaneous generation of both EMIC (ion) and chorus (electron) waves. The EMIC waves had maximum wave amplitudes of ~6 nT in a ~60 nT ambient field B_0. The observed EMIC wave amplitudes were about ~10 times higher than the usually observed chorus amplitudes (~0.1–0.5 nT). The EMIC waves are found to be coherent to quasi-coherent in nature. Calculations of relativistic ~1–2 MeV electron pitch angle transport are made using the measured wave amplitudes and wave packet lengths. Wave coherency was assumed. Calculations show that in a ~25–50 ms interaction with an EMIC wave packet, relativistic electron can be transported ~27° in pitch. Assuming dipole magnetic field lines for a $L = 9$ case, the cyclotron resonant interaction is terminated ~±20° away from the magnetic equator due to lack of resonance at higher latitudes. It is concluded that relativistic electron anomalous cyclotron resonant interactions with coherent EMIC waves near the equatorial plane is an excellent loss mechanism for these particles. It is also shown that $E > 1$ MeV electrons cyclotron resonating with coherent chorus is an unlikely mechanism for relativistic microbursts. Temporal structures of ~30 keV precipitating protons will be ~2–3 s which will be measurable at the top of the ionosphere.

1. Introduction

Electromagnetic ion cyclotron (EMIC) waves (0.1–5 Hz) are generated by $T_\perp/T_\parallel > 1$ anisotropic 10–100 keV protons [*Cornwall*, 1965; *Kennel and Petschek*, 1966], where $T_\perp$ and $T_\parallel$ indicate the perpendicular and parallel particle temperatures relative to the background magnetic field B_0, respectively. The general scenario for the generation of these waves is injection of the energetic ions from the nightside plasma sheet during magnetic storms or substorms [*Cornwall and Schulz*, 1971; *Vasyliunas*, 1975]. The particles are thought to go most unstable when their gradient and curvature drift into the duskside plasmaspheric bulge, where the wave phase speed is the lowest [*Thorne and Kennel*, 1971; *Fraser and McPherron*, 1982; *Horne and Thorne*, 1998; *Meredith et al.*, 2003; *Halford et al.*, 2010]. EMIC waves are greatly enhanced during magnetic storms with typical wave amplitudes in the range 1–10 nT [*Erlandson and Ukhorskiy*, 2001; *Turner et al.*, 2014].

In a similar way, magnetospheric electromagnetic chorus (100 Hz–10 kHz) is generated by anisotropic 10–100 keV electrons with $T_\perp/T_\parallel > 1$ [*Kennel and Petschek*, 1966; *Tsurutani et al.*, 1979]. The typical source of these electrons and their anisotropies are the same as for protons, particle injection from the nightside plasma sheet during magnetic storms [*Tsurutani et al.*, 1975; *Delport et al.*, 2012], or substorms [*Thorne et al.*, 1974, 1977; *Tsurutani and Smith*, 1974, 1977; *Hayakawa et al.*, 1986; *Koons and Roeder*, 1990; *Meredith et al.*, 2001, 2012; *Li et al.*, 2013]. However, electrons drift from midnight through dawn, in the opposite sense as the protons. It has been shown that chorus is generated close to the geomagnetic equatorial plane or in minimum B field pockets [*Tsurutani and Smith*, 1974, 1977; *LeDocq et al.*, 1998; *Lauben et al.*, 2002; *Omura et al.*, 2008] by the electron temperature anisotropy instability [*Kennel and Petschek*, 1966; *Tsurutani and Lakhina*, 1997].

Energetic electrons drift from midnight through dawn to noon, and chorus is typically observed in these local time sectors [*Thorne et al.*, 1974; *Tsurutani and Smith*, 1977; *Verkhoglyadova et al.*, 2009]. Chorus is most frequently observed at local dawn. The physical cause of chorus from dawn to noon is believed to be the upwelling of plasma due to sunlight heating of the upper atmosphere. This leads to the lowering of the local wave phase speed and thus enhancement of the instability [*Brice and Lucas*, 1971; *Jentsch*, 1976; *Tsurutani and Smith*, 1977]. This is the same mechanism as for protons, but on the opposite side of the magnetosphere.

Another possible means of generating energetic proton and electron temperature anisotropies is by the impingement of interplanetary shocks [*Olson and Lee*, 1983; *Kennel et al.*, 1985; *Papadopoulos*, 1985; *Tsurutani et al.*, 1988] or other types of solar wind pressure pulses onto the magnetosphere. Fast forward shocks have density jumps comparable to their magnetosonic Mach numbers [*Kennel et al.*, 1985; *Tsurutani et al.*, 2011a] and thus the enhanced ram pressure leads to a rapid compression of the magnetosphere. As the pressure pulse hits the magnetosphere, betatron acceleration of remnant 10–100 keV protons and electrons will have their perpendicular temperatures raised and thus their temperature anisotropies $T_{\perp} > T_{\parallel}$ increased, possibly leading to plasma instabilities.

We have selected a high solar wind pressure event during the Cassini near-Earth flyby on 18 August 1999 to study this type of event in detail. Cassini flew close to the Sun-Earth line through the dayside magnetosphere. The Cassini magnetic field wave data will be analyzed in detail. Section 2 describes the data used and the methodology for wave mode analyses used in this work. Section 3 gives the interplanetary conditions during the event, a detailed analysis of proton cyclotron waves and the occurrence of whistler mode chorus waves. Cyclotron resonant wave-particle interactions and the pitch angle transport of relativistic electrons by the EMIC waves are calculated in section 4. Sections 5 and 6 give a brief discussion of the results and concluding remarks.

2. Data and Analysis Method

2.1. Satellite Trajectory and Data

Figure 1 displays the trajectories of the Cassini spacecraft during the Cassini near-Earth flyby. The trajectories are in GSM (geocentric solar magnetospheric) coordinates in the (top) *X*-*Y* and (bottom) *X*-*Z* planes. The GSM coordinate system has its *X* axis from the Earth to the Sun and the *Y* axis defined to be perpendicular to the Earth's magnetic dipole so that the *X*-*Z* plane contains the dipole axis. The positive *Z* axis is chosen to be in the same sense as the magnetic pole (positive north). Hours in *UT* are marked along the trajectory in the figure. Model bow shock and magnetopause locations are also marked in the background. Cassini-Huygens flew past Earth on 18 August 1999, on its way to Saturn with a unique trajectory through the subsolar point of the Earth's magnetosheath and magnetosphere. The flyby along the Sun-Earth line provided an opportunity to study the magnetospheric plasma waves in detail. Our study considers the time interval 0226 UT to 0240 UT, 18 August 1999, when Cassini was in the Earth's outer magnetosphere. The satellite crossed L shells from $L = 10$ to $L = 7$ near the magnetic equator from 3.1°–1.5° magnetic latitude (MLAT), an ideal trajectory to possibly detect ion and electron plasma waves.

The 32 sample/second high sampling rate fluxgate magnetometer data from Cassini is used to identify the wave events present in the Earth's outer magnetosphere. Chorus waves are identified from the Cassini RPWS (Radio and Plasma Wave Science) search coil magnetometer data. The solar wind and interplanetary magnetic field data at 1 min time resolution are obtained from the OMNI website (http://omniweb.gsfc.nasa.gov/). The interplanetary convection time from the spacecraft to the magnetopause has already been time adjusted; hence, no further adjustments were made to the OMNI data used in this study. One minute *AE* indices and 1 h *Dst* data were obtained from the World Data Center for Geomagnetism, Kyoto, Japan (http://wdc.kugi.kyoto-u.ac.jp/). The integrated fluxes of electrons with energies $E > 2.0$ MeV were collected by the Geostationary Operational Environment Satellites instrumentation (GOES-8) (http://www.ngdc.noaa.gov/stp/satellite/goes/dataaccess.html).

2.2. Methodology

A new program called the Rosetta Automatic Wave Analysis (RAWA) has been developed to analyze the plasma waves in space plasma regions [*Tsurutani et al.*, 2013a; *Remya et al.*, 2014]. The raw magnetic field vectors are first low-pass filtered. A Butterworth filter was used. A cutoff value for the Cassini wave interval of 30 mHz was applied. This cutoff frequency was below the dominant power region of the waves. The low-pass values are used for the background magnetic fields and the high-pass-filtered data are used as the wave fields.

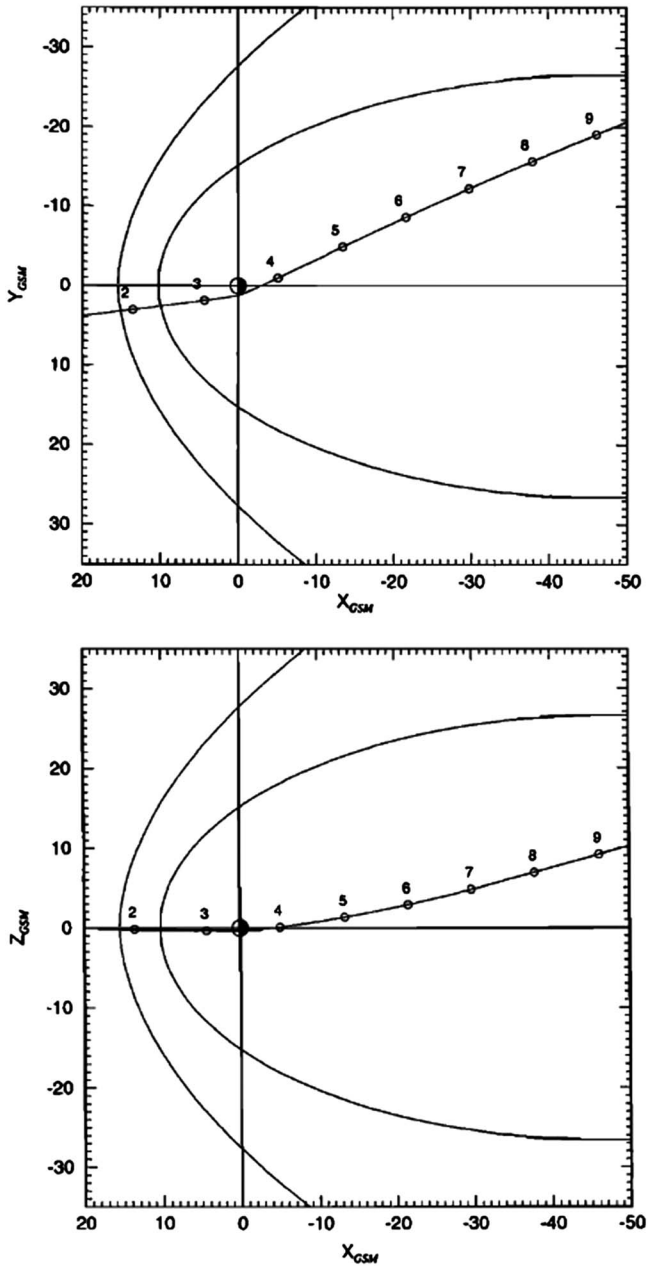

Figure 1. Cassini Earth swing-by trajectory projected onto (top) the GSM *X-Y* equatorial plane and (bottom) the GSM *X-Z* noon-meridian plane. Hours in *UT* are marked along the trajectory. Model bow shock and magnetopause locations are also shown. (taken from *Southwood et al.* [2001, Figure 1]).

Wave cycles are selected from the high-pass-filtered data, and minimum variance analysis (MVA) [*Sonnerup and Cahill Jr.*, 1967; *Smith and Tsurutani*, 1976] is performed on individual wave cycles. Eigenvalues λ_1, λ_2, and λ_3 and their corresponding eigenvectors are calculated. The eigenvectors represent the maximum, intermediate, and minimum variance directions of the field components. The wave magnetic fields are rotated into minimum variance coordinates $\vec{B}_1$, $\vec{B}_2$, and $\vec{B}_3$, where the $\vec{B}_3$ vector points along the direction of minimum variance and hence the direction of the wave vector $\vec{k}$ (with 180° ambiguity) [*Verkhoglyadova et al.*, 2010]. See section 2 of *Remya et al.* [2014] for the detailed analysis technique.

The frequencies and polarizations derived using the above technique are in the spacecraft (s/c) reference system. Since the present study focuses on the magnetosphere where the plasma flow speed is quite low compared to the wave phase speed, the wave frequency Doppler shift is negligible and can be ignored. The

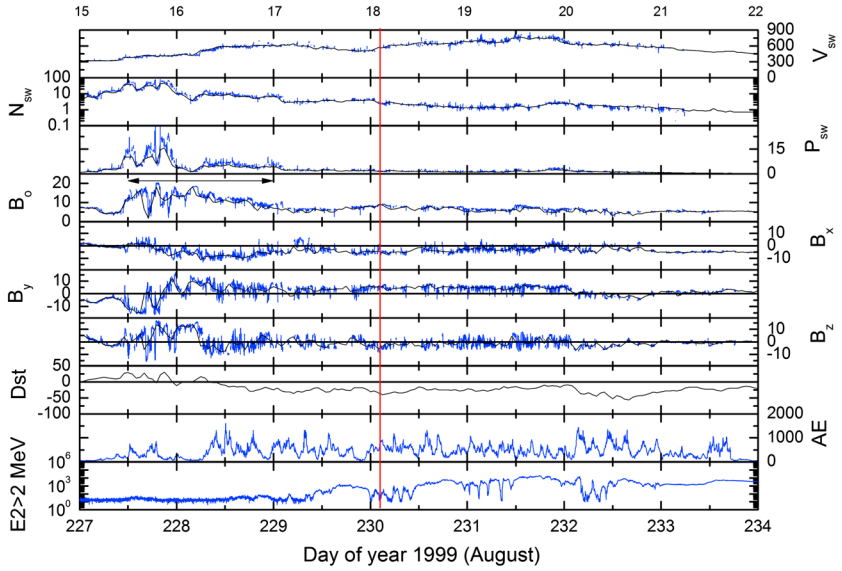

Figure 2. Interplanetary and geomagnetic parameters during 15–22 August 1999 (day of year (DOY) 227–234). From top to bottom, the panels show the variations of (first panel) solar wind speed (V_{sw} in km s^{-1}), (second panel) plasma density (N_{sw} in cm^{-3}), (third panel) solar wind ram pressure (P_{sw} in nPa), IMF magnitude (fourth panel) (B_0 in nT) and (fifth panel) B_x (nT), (sixth panel) B_y (nT) and (seventh panel) B_z (nT) components in the GSM coordinate system, and the (eighth panel) *Dst* (nT) and (ninth panel) *AE* (nT) indices, and (tenth panel) $E > 2$ MeV relativistic electron fluxes (cm^{-2} s^{-1} sr^{-1}) from GOES-8, respectively. The blue and black curves are 1 min and 1 h time resolution data, respectively. In the B_0 panel, the horizontal arrow indicates the CIR interval from middle of 15 August to end of 16 August. The vertical red line at 0226 UT, 18 August is the time of the wave event.

frequencies and polarization measured in the spacecraft frame will be the same as those in the plasma frame, to first order. The direction of the magnetic field is automatically incorporated into the minimum variance hodograms so the wave handedness can be easily visualized.

The wave coherency has been examined. Groups of wave cycles (wave packets) are selected from the wave data. The B_1 and B_2 wave components are cross correlated to determine the level of wave coherency. Highly coherent waves will have a cross-correlation coefficient of 1.0 at approximately zero ($\frac{1}{4}$ wavelength) lag and $\geq$0.95 at $\pm$1 lag. For example, see *Tsurutani et al.* [2011b] for highly coherent electromagnetic chorus in the Earth's magnetosphere. For lesser coherent waves, the peak correlation coefficient at zero lag can be significantly less than 1.0 (say 0.5) with further decrease in correlation coefficient values at larger lags. Waves with these characteristics have been called "quasi-coherent". Incoherent turbulence will have little or no correlation between the B_1 and B_2 wave components.

3. Magnetospheric Waves

3.1. Interplanetary Conditions

We examine different interplanetary parameters upstream of the interplanetary shocks to identify the conditions under which the magnetospheric waves were generated. This is shown in Figure 2. From top to bottom are the solar wind speed, the density, solar wind ram pressure, magnetic field magnitude, and the three components of the field in GSM coordinates. The two panels near the bottom are the *Dst* and *AE* geomagnetic indices. Figure 2 (tenth panel) is the $E > 2$ MeV electron flux. The entire interval of 15–22 August 1999 is shown so that the reader can see the conditions before, during, and after the wave events.

This is a typical high-speed solar wind interval [*Tsurutani et al.*, 1995, 2006]. The solar wind starts at 300 km/s at the beginning of day 227 and increases to a peak speed of ~756 km/s at 1239 UT on day 231. A corotating interaction region (CIR) [*Smith and Wolfe*, 1976; *Pizzo*, 1985; *Balogh et al.*, 1999] is present from 1043 UT day 227 to 00 UT day 229. This structure is indicated by a horizontal arrow in the B_0 panel. The CIR does not cause a magnetic storm in this case. The *Dst* value stays well above > -50 nT.

During the remainder of the high-speed stream from 00 UT day 229 to day 231, there are large-amplitude IMF (interplanetary magnetic field) B_z fluctuations (fourth panel from the bottom). These are the outward

propagating Alfvén waves which are embedded within the solar wind [*Belcher and Davis*, 1971]. Intense auroral activity occurs during the high-speed stream proper. The activity is nearly continuous from the beginning of 17 August until the end of 21 August. Although this interval does not follow all of the four "strict" criteria of high-intensity, long-duration, continuous AE activity (HILDCAA) [*Tsurutani and Gonzalez*, 1987], the long-duration and intense auroral activity seems to be remarkable. This geomagnetic activity is caused by sporadic magnetic reconnection [*Dungey*, 1961; *Gonzalez and Mozer*, 1974] between the southward components of the IMF B_z components of the Alfvén waves and the Earth's northward dayside magnetopause magnetic field.

The high auroral activity interval is associated with enhancements in the fluxes of relativistic $E > 2$ MeV electrons at the geosynchronous orbit, shown in Figure 2 (tenth panel). The flux enhancement exhibits a lag of ~1.5 days from the initiation of intense auroral activity. This is in agreement with the findings of *Hajra et al.* [2013, 2014, 2015].

The Alfvén wave negative B_z components cause dayside magnetic reconnection at the Earth's dayside magnetopause. Subsequent nightside reconnection in the form of substorm/convection events cause the injection of energetic ~10–100 keV electrons into the nightside magnetosphere [*DeForest and McIlwain*, 1971; *Horne and Thorne*, 1998]. The temperature anisotropy of the heated electrons leads to plasma instability [*Kennel and Petschek*, 1966], generating electromagnetic plasma waves called "chorus." Resonant interactions of the chorus with ~100 keV electrons lead to their acceleration to relativistic energies [*Inan et al.*, 1978; *Horne and Thorne*, 1998; *Thorne et al.*, 2005; *Summers et al.*, 2007b; *Thorne et al.*, 2013].

The interval of the waves under study (red vertical line) is an interval with a slight solar wind speed increase (Figure 2, first panel) and slight solar wind density decrease (Figure 2, second panel). The overall solar wind pressure (Figure 2, third panel) is more or less constant. Any pressure variations must be due to small solar wind fluctuations that have temporal scales smaller than those shown here. The relativistic $E > 2$ MeV fluxes have a minor decrease at the time of the wave events.

3.2. Proton Cyclotron Waves

Figure 3 displays the magnetic field components in GSM coordinates. This interval (0226–0240 UT) corresponds to the outer region of the dayside subsolar magnetosphere from $L = 9.9$ to $L = 7$. The magnetopause was located at L ~10.0. The magnetic field magnitude increases from ~45 nT at the magnetopause crossing (~0226 UT) to ~72 nT in the magnetosphere at ~0239 UT. At ~0227 UT the transverse wave amplitudes are ~6 nT. The ambient magnetic field is ~60 nT. The satellite was close to the magnetic equator and covered 3.1°–1.5° MLAT during this interval.

As described previously, the magnetic data were filtered, keeping both the low-pass and high-pass parts of the data. These are presented in Figures 4 and 5, respectively. Figure 4 shows the low-pass data. This is used for both the ambient magnetic field direction and also for its magnitude. The first will be used to calculate the wave $\vec{k}$ direction relative to B_0 and the second for the instantaneous ion cyclotron frequency. The data in Figure 5 are used for the detailed wave analyses. Wave cycles are identified from this high-pass data, and MVA are applied on individual cycles for wave mode analyses.

Figure 6 shows some pertinent results from the minimum variance analyses performed on various individual wave cycles. The ratio λ_1/λ_2 is the ratio of the maximum to intermediate eigenvectors. A value of 1.0 indicates circular polarization and infinity, linear polarization. The angle θ_{kB_0} is the angle of wave propagation relative to the ambient magnetic field. The sense of rotation or polarization in the spacecraft frame (same as the plasma frame) is also given in the panels corresponding to individual cycles. The direction of the ambient magnetic field is set such that it always points "out" of the plane and is indicated by the symbol "O" in each panel of the figure. LH(E)/RH(E) indicates left-hand circular (elliptical)/right-hand circular (elliptical) polarizations. The beginnings and ends of each wave cycle are indicated by "b" and "e," respectively. This is done so that the reader can easily identify the clockwise or anticlockwise rotation of the wave.

Figure 6 gives the wave cycles for 0229:06.4–0229:08.4 UT (top left), 0229:53.1–0229:54.9 UT (top right), 0232:20.1–0232:22.8 UT (middle left), 0232:20.1–0232:22.8 UT (middle right), 0237:07.9–0237:10.8 UT (bottom left), and 0237:35.9–0237:38.5 UT (bottom right). The wave cycles shown are all LH polarized. The waves are circularly to slightly elliptically polarized. The waves are determined to be propagating parallel/quasi-parallel ($\theta_{kB_0} < 30^o$) to the ambient magnetic field.

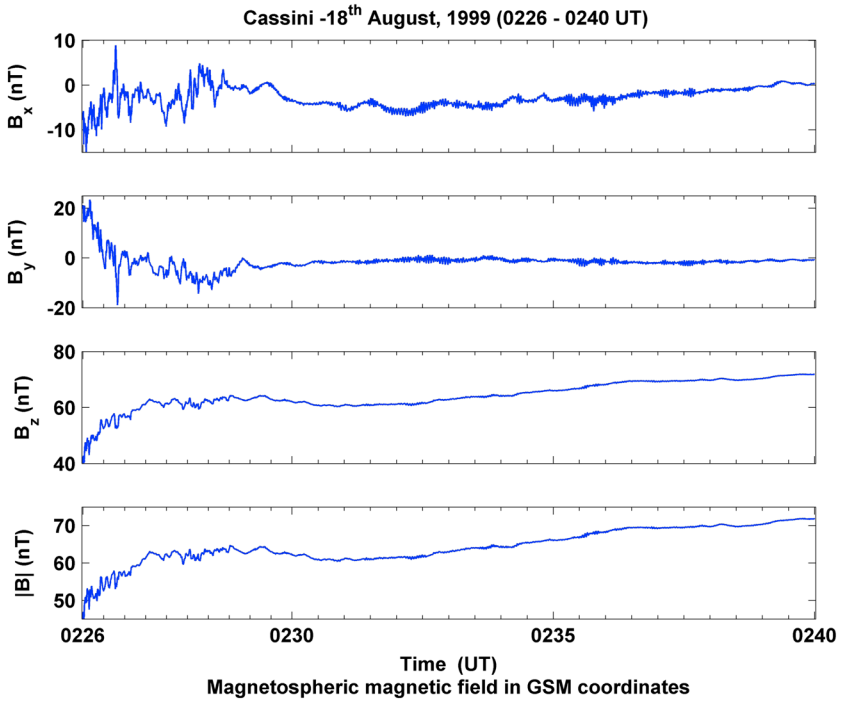

Figure 3. Cassini: Temporal behavior of the Earth's magnetospheric magnetic field in GSM coordinates for the interval 02:26–02:40 UT on 18 August 1999.

A total of 99 wave cycles were analyzed from the data set. A total of 77/99 (~78%) of the waves were found to be left-hand (LH) polarized, approximately 21% (21/99) were right-hand (RH) polarized, and about ~1% (1/99) was linearly polarized. The remainder of the analyses and discussion will be devoted to the LH-polarized waves. Analysis of the RH waves will be postponed for a later publication.

A histogram of θ_{kB_0} is presented in Figure 7a for the LH waves. The majority of the waves (~78%) were propagating parallel/quasi-parallel ($\theta_{kB_0} < 30°$) to the ambient magnetic field, ~22% with $30° < \theta_{kB_0} < 60°$. Only one event had $\theta_{kB_0} > 60°$. The waves were circular to elliptically polarized.

Figure 7b depicts the histogram of the LH wave frequency, normalized to proton gyrofrequency f_{cp}. The observed waves were found to have frequencies less than or close to proton (ion) cyclotron frequency (f_{cp}) in the spacecraft frame with maximum distribution around half the proton gyrofrequency $f_{cp}/2$. It can be concluded from this result and the others that the LH-polarized waves are propagating in the ion cyclotron mode.

The waves analyzed were found to be compressional. The compression factors are calculated using the relationship $(B_{max} - B_{min})/B_{max}$ where B_{max} and B_{min} are the maximum and minimum field magnitudes, respectively. The compression factors as described above varied between 0.3 and 0.9 relative to the wave amplitude.

Figure 8 shows the coherence of the EMIC waves. The figure shows $B_1 - B_2$ components of Cassini waves for the time interval 0232:17.5–0232:47.3. The wave packet duration is ~30 s. Figure 8 (top) gives the B_1 and B_2 values as a function of time. Figure 8 (bottom) displays the $B_1 - B_2$ cross-correlation result. The peak correlation coefficient is 0.78 at ~ −320° lag and decreases with greater lags. In comparison to magnetospheric chorus at the equator [*Tsurutani et al.*, 2011b], we would say that the Cassini ion cyclotron waves are close to coherent or are quasi-coherent in nature.

3.3. Whistler Mode Chorus Emissions

Figure 9 shows the dynamic spectra of the magnetic field component B_y in the magnetosphere during the interval 0226–0240 UT, 18 August 1999. Figure 9a plots the magnetic frequency-time spectrogram for fluxgate magnetometer data covering frequencies up to 4 Hz. The magnetic spectral density is plotted as a function of frequency and time according to the color bar provided at the right side of the figure. The

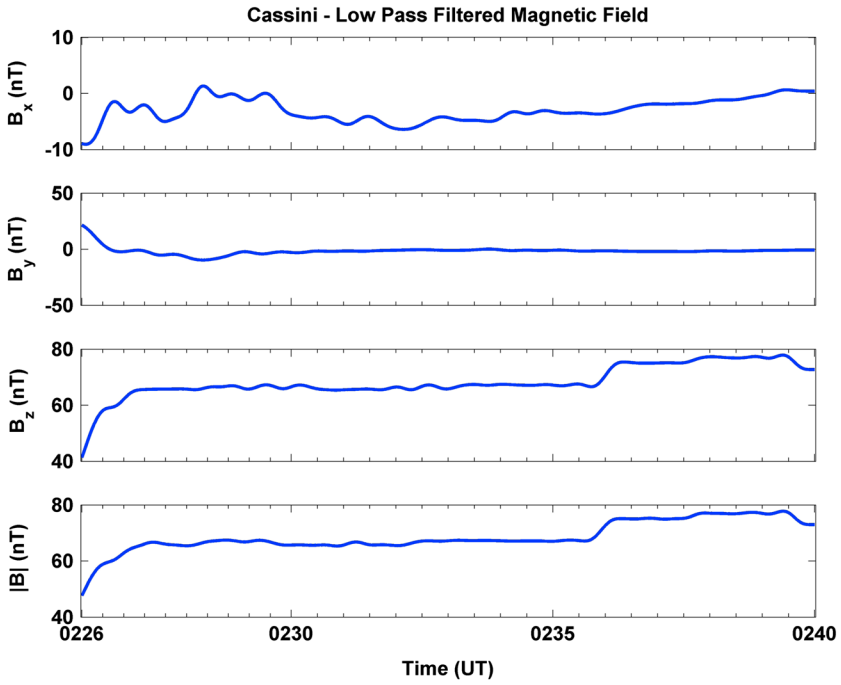

Figure 4. Background magnetic field obtained after a low-pass filtering of the raw data at 30 mHz.

magenta, green, blue, and black lines, respectively, indicate the proton (H^+), He^{2+}, He^+, and O^+ cyclotron frequencies. The figure clearly shows the presence of ion cyclotron waves with frequencies less than or close to half the proton gyrofrequency. The strong wave bursts are observed at frequencies between the He^{2+} and He^+ cyclotron frequencies. It could be because the He^{2+} and He^+ stop bands are limiting the frequency range of the observed proton cyclotron waves. *Matsuda et al.* [2014] have indicated the possible presence of He^{2+} ions in substantial quantities inside the plasmasphere to create a He^{2+} stop band there. At this time the amount

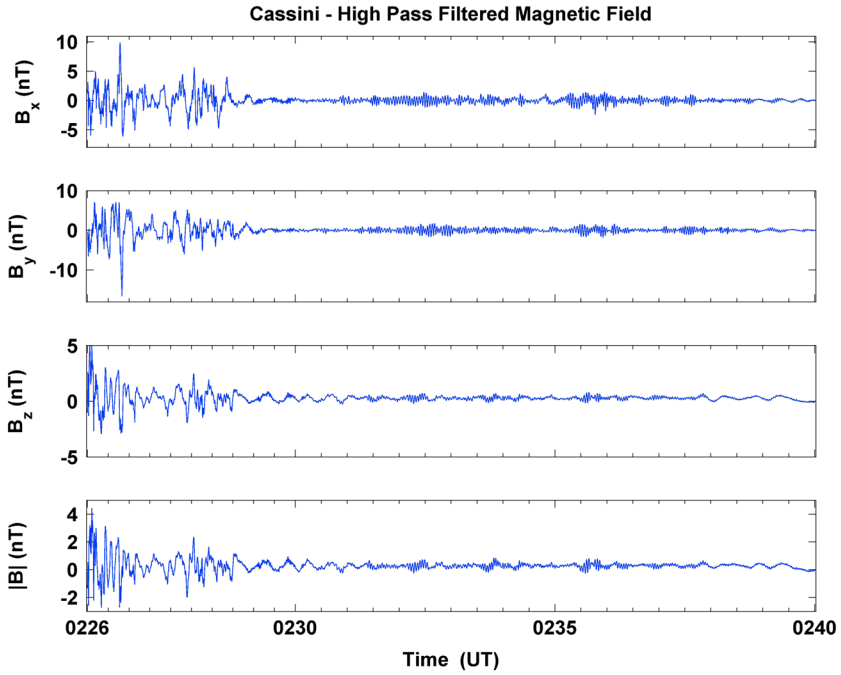

Figure 5. Magnetospheric wave fields obtained from Cassini after the removal of low-pass data.

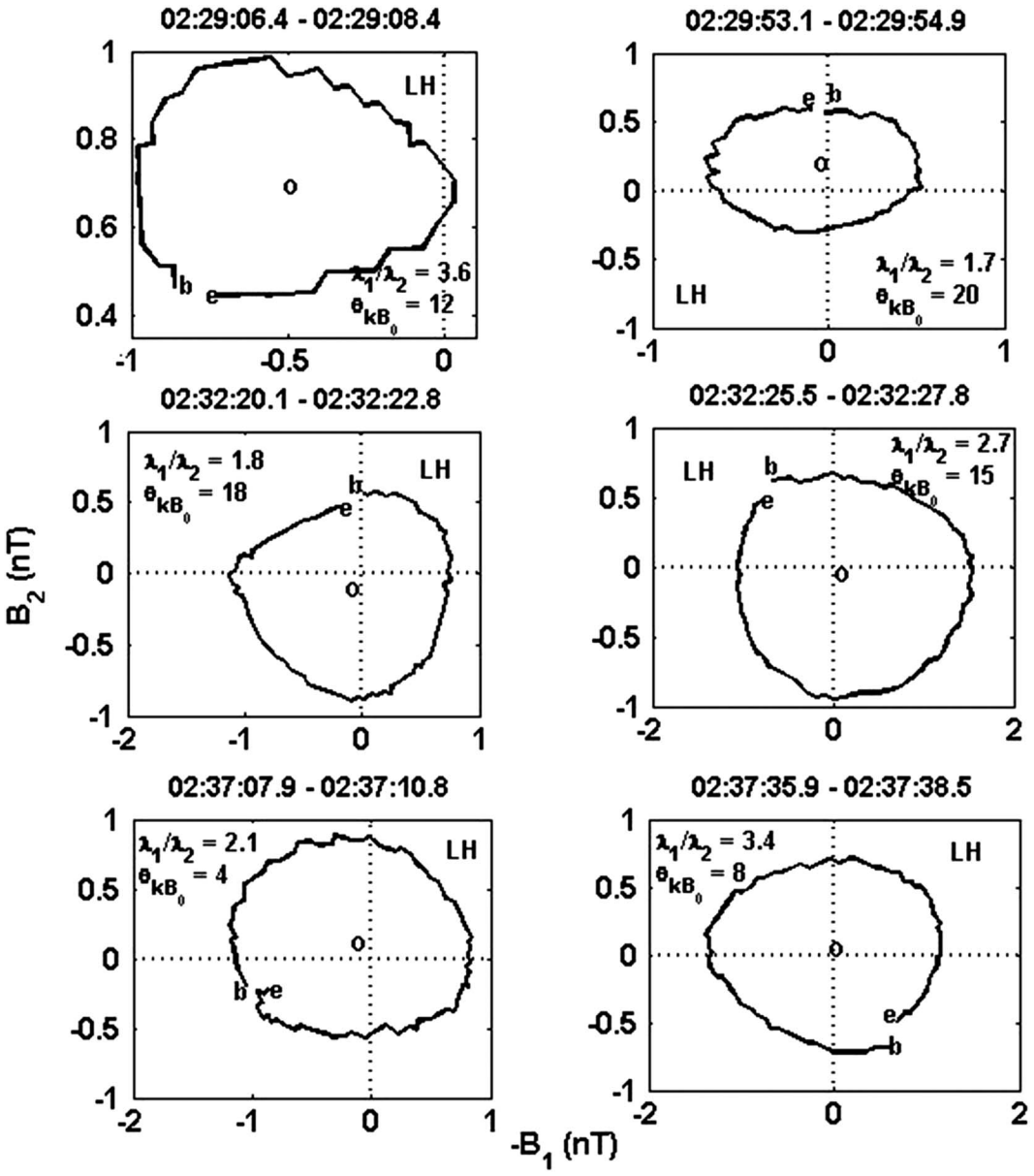

Figure 6. Cassini: Hodograms of the magnetospheric wave cycles in minimum variance coordinates for the interval 0226–0240 UT.

of He^{2+} in the outer magnetosphere is unknown. However, another possibility for the reduced amplitude of the waves close to $f_{cHe^{2+}}$ or $f_{cp}/2$ could be due to Landau damping, much in the way possible damping of chorus at $f_{ce}/2$ causes two-frequency chorus [*Tsurutani and Smith*, 1974]. The magnetopause crossing was at 0226 UT ($L = 9.9$) and the strong bursts that appear before 0230 UT are the magnetopause boundary layer waves. To first order, we do not observe any obvious EMIC rising tones.

Figure 9b depicts the Cassini search coil data in the same format as above for frequencies up to 2.5 kHz. The instrument mode used for the flyby was designed to concentrate on the 2.5 kHz waveform measurements which can be used to validate the wave normal analysis of whistler mode waves. A red line is used to trace the electron cyclotron frequency f_{ce} in the figure. The spectrum clearly indicates patches of whistler mode electromagnetic chorus emissions at frequencies below f_{ce}. Chorus structures were prominent at 0229–0235 UT. These rising tone chorus shown here were detected at ~1300 MLT (magnetic local time) at

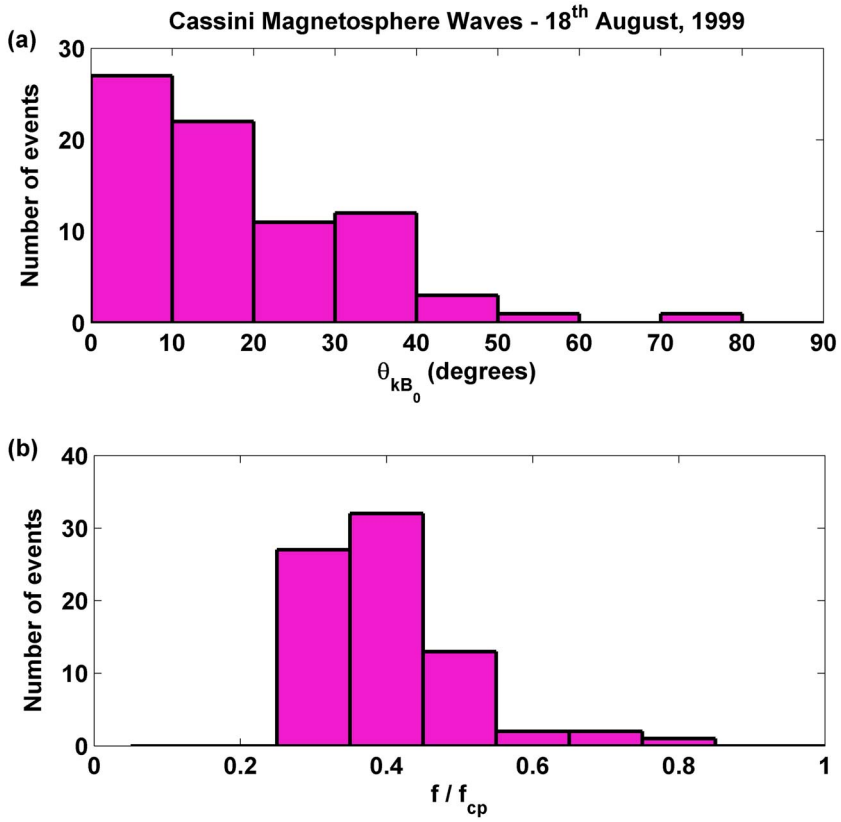

Figure 7. (a) Distribution of the magnetosphere wave propagation directions with respect to the background magnetic field (b) Histogram of the wave frequencies normalized to proton cyclotron frequency, f/f_{cp}.

$L = 9.3$. The chorus waves were detected quite close to the equatorial generation region, 2.7° MLAT as has been discussed earlier.

4. Resonant Wave-Particle Interactions

When a particle senses that an electromagnetic wave Doppler shifted to its cyclotron frequency or its harmonics, it can resonate with the waves to either gain or lose pitch angle. The cyclotron resonance condition for wave-particle interaction is given by the following [*Kennel and Petschek*, 1966]:

$$\omega - k_{\|} v_{\|} = \frac{n\Omega}{\gamma} \tag{1}$$

where ω is the wave frequency, $k_{\|}$ and $v_{\|}$ are the components of the wave vector **k** and particle velocity **v**, parallel to the ambient field $\mathbf{B}_0$, respectively. In the above, Ω is the particle cyclotron frequency in radians/sec, n is the harmonic number ($= 0, \pm 1, \pm 2, \ldots$), and $\gamma = (1 - v^2/c^2)^{-\frac{1}{2}}$ is the relativistic factor. In the expression for γ, v is the particle speed and c is the speed of light. For positive (negative) values of n, equation (1) represents the normal (anomalous) cyclotron resonance condition [*Tsurutani and Lakhina*, 1997]. For normal ($n = 1, 2, 3, \ldots$) Doppler shifted cyclotron resonance, the waves and particles travel in opposite directions from each other along the magnetic field and the waves will be Doppler shifted up to the particle cyclotron frequency or its harmonics in the proton reference frame. In case of anomalous resonance ($n = -1, -2, -3, \ldots$), the waves and particles travel in the same direction with the particles overtaking the waves. The particles sense the waves to have a polarization opposite to the plasma frame polarization. Since the particles interact with the opposite polarization waves the term "anomalous" cyclotron resonance has been used to describe this interaction. For example, ions interact with RH waves and sense them as LH polarized and vice versa, electrons interact with LH waves and sense them as RH. However, in the later case, because the LH waves have frequencies much below the electron cyclotron frequencies, resonant electrons must have relativistic parallel kinetic energies ($E_{\|} >$ MeV) [*Tsurutani and Lakhina*, 1997].

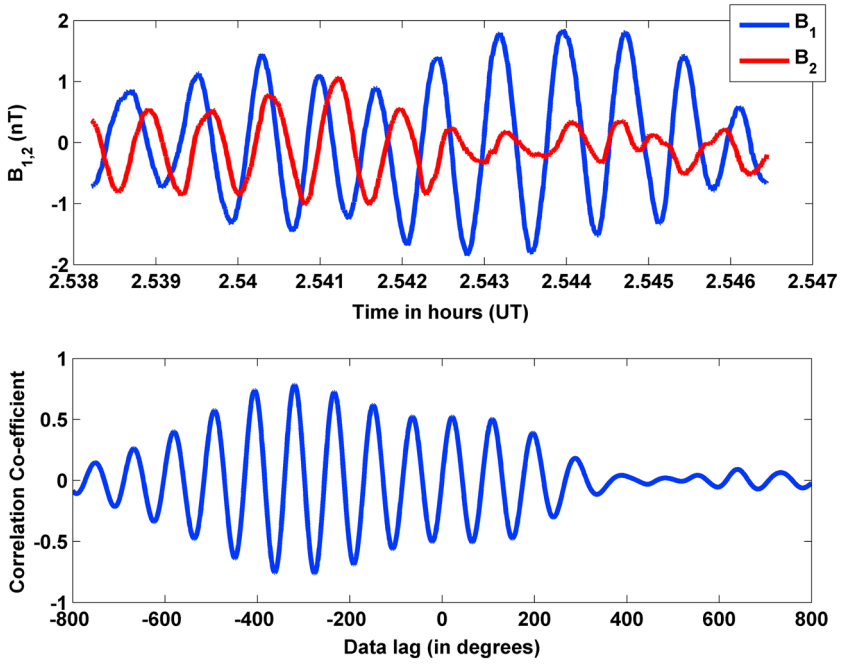

Figure 8. (top) The $B_1 - B_2$ components of Cassini waves for the interval 0232:17.5–0232:47.3. (bottom) The correlation coefficient at various data point lags. Peak correlation coefficient is 0.78 at lag −320°.

For the fundamental anomalous electron cyclotron resonance ($n = -1$) with a left-hand wave, equation (1) can be simplified for resonant particle velocity:

$$v_{\parallel} = v_{\parallel R} = v_{\mathrm{ph}}(1 + \Omega/\omega\gamma) \tag{2}$$

where v_{ph} is the parallel wave phase speed. The relativistic parallel kinetic energy of the resonant electrons is thus given by

$$E_{\parallel R} = \frac{\gamma m v_{\parallel R}^2}{2} = \frac{\gamma m v_{\mathrm{ph}}^2}{2}(1 + \Omega/\omega\gamma)^2 \tag{3}$$

The particle pitch angle scattering rates due to incoherent electromagnetic or electrostatic waves have been derived by *Kennel and Petschek* [1966] and *Tsurutani and Lakhina* [1997]. However, since the observed EMIC waves are coherent or quasi-coherent, the wave-particle interaction is considerably stronger. The energetic electrons will stay in gyroresonance with the wave for more than a wave cycle and may undergo large pitch angle changes in a single wave-particle encounter. This process has been called pitch angle transport [*Tsurutani et al.*, 2009; *Lakhina et al.*, 2010]. In this paper we try to obtain pitch angle scattering rates for EMIC waves from simple physical arguments assuming wave coherence [*Tsurutani et al.*, 2011b].

4.1. Pitch Angle Scattering

The change in the particle pitch angle α of electrons which are in cyclotron resonance with the electromagnetic ion cyclotron waves can be obtained from the following: $\tan\alpha = v_{\perp}/v_{\parallel}$, where α is the angle between the particle velocity vector **v** and the ambient field $\mathbf{B}_0$ and $v_{\perp}$ is the perpendicular component of the particle velocity with respect to $\mathbf{B}_0$. The pitch angle diffusion rates for small pitch angles is identical to the expression for the diffusion rates for large pitch angles [*Kennel and Petschek*, 1966; *Tsurutani and Lakhina*, 1997]. The change $\Delta\alpha$ in particle pitch angle for arbitrary α is obtained as follows:

$$\Delta\alpha = \frac{B}{B_0}\Omega\Delta t \tag{4}$$

The pitch angle diffusion rate is obtained to be [*Tsurutani and Lakhina*, 1997; *Tsurutani et al.*, 2009]

$$D = \frac{(\Delta\alpha)^2}{2\Delta t} = \frac{\Omega}{2}\left(\frac{B}{B_0}\right)^2\eta \tag{5}$$

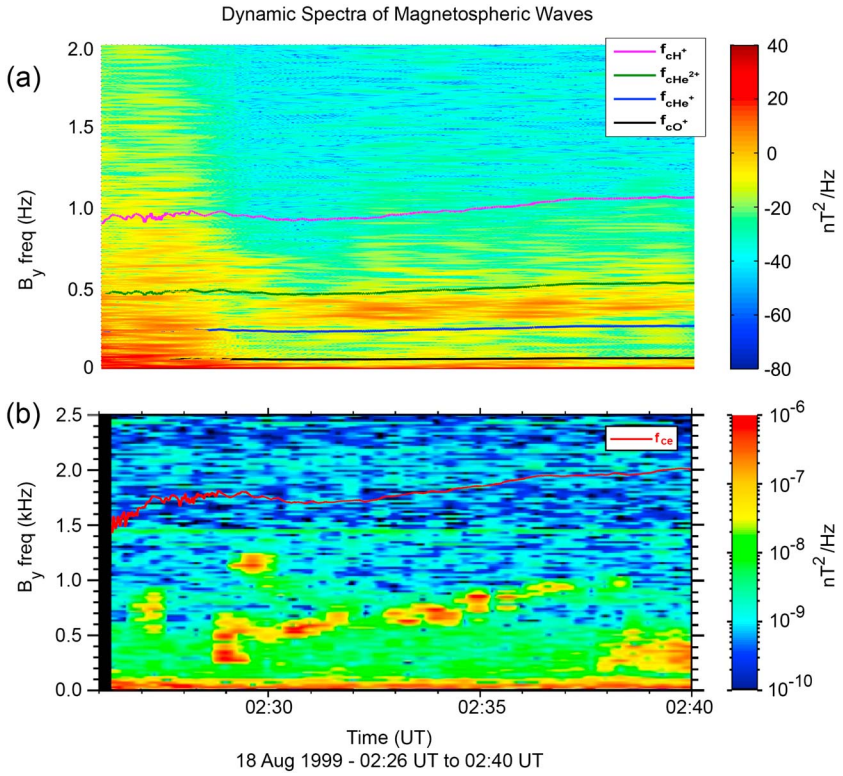

Figure 9. The dynamic power spectra for the magnetospheric magnetic field observed by (a) Cassini MAG and (b) Cassini Radio and Plasma Wave Science (RPWS) during the Earth flyby. Figure 9a shows the proton cyclotron waves and Figure 9b indicates presence of whistler mode chorus structures.

where $\eta = \Omega\Delta t$ is the fractional amount of time that the particle is in resonance with the wave. In the above expressions, Ω is the electron cyclotron frequency and Δt is the interaction time between the electrons and the wave packet.

For the electromagnetic proton cyclotron wave packet considered in Figure 8, we have the following values: frequency $\omega = 2.25$ rad/s, electron gyrofrequency $\Omega_e = 1.08 \times 10^4$ rad/s, and wave packet amplitude $B = 0.44$ nT in an ambient field of magnitude $B_0 \sim 62$ nT. The wave is detected at $L = 9$ and at a geomagnetic latitude 2.6°. The wave phase speed of the proton cyclotron wave is obtained to be $v_{ph} \simeq 2.2 \times 10^5$ m/s by numerical calculations using the Waves in Homogeneous Anisotropic Magnetized Plasma code [*Ronnmark*, 1982]. By successive iteration using the Newton-Raphson method [*Gerald and Wheatley*, 2004], the resonant electron parallel speed is determined to be $v_{\|} \simeq 2.88 \times 10^8$ m/s. The Newton-Raphson method uses the first few terms of the Taylor series of a function in the vicinity of a suspected root. The relativistic factor γ is calculated to be 3.7. The proton cyclotron wave packet duration is 29.7 s (10 wave cycles) in the spacecraft frame. It is assumed that the electrons stay in resonance with the wave while passing through the packet. Assuming the above wave speed, the wave packet spatial length X is obtained as the wave phase speed times the wave packet duration. The wave packet spatial size is therefore $X \simeq 6.5 \times 10^6$ m. The interaction time between the electrons and the wave packet is the spatial length of the wave packet divided by the relative speed of the electrons with the wave packet. The interaction time is $\Delta t = 22.6$ ms. The electron pitch angle transport obtained is $\Delta\alpha = 0.48$ radians or ~27° in this single interaction. In the above, we have used the relativistic electron mass for obtaining Ω_e in equation (4). The maximum diffusion rate is thus obtained to be $D = 5.1\ s^{-1}$ for multiple wave packet interactions. The time of diffusion is $T = 1/D \simeq 195$ ms. If the relativistic electron stays in resonance with the whole proton cyclotron wave packet (~ 23 ms), then the electrons can be pitch angle transported 27° in this interaction. Electrons could have several interactions with wave packets during a single pass through the wave region, and the angular transport/scattering could be even greater. Note that the coherent waves shown here and used in the pitch angle transport calculations were for 0.44 nT wave amplitudes. If the higher amplitude waves are used, the transport will be substantially higher.

Table 1. Pitch Angle Scattering at Various L Shells

	v_{ph} $\times 10^5$ (m/s)	Ω_e $\times 10^4$ (rad/s)	ω (rad/s)	$v_{\|\|}$ $\times 10^8$ (m/s)	γ	$E_{\|\|}$ (MeV)	Δt (ms)	$\Delta\alpha$ (deg)	D (s^{-1})	T (ms)
$L = 10$	2.26	1.077	3.1	2.803	2.8	0.625	48.3	66	13.8	72
$L = 9$	2.19	1.08	2.25	2.88	3.66	0.87	22.6	27	5.12	195
$L = 8$	2.32	1.3	2.6	2.904	3.98	0.954	46.2	25	2.12	472
$L = 7$[a]	2.37	1.48	3	2.906	4.02	0.965	24.5	24	3.75	267
$L = 6$[a]	3.49	3.43	3	2.99	13.4	3.4	35.1	11	0.485	2060

[a]No waves were observed at these L values. Frequency, amplitude, and wave packet duration are assumed values and are given in the text.

How does this compare to the pitch angle transport of relativistic electrons with coherent chorus? The numbers have not been derived for relativistic electrons but have been done for ~23 keV electrons [*Tsurutani et al.*, 2009]. It has been shown for a specific wave example, ~23 keV electrons could cyclotron resonate with ~0.25 f_{ce} chorus where the wave phase speed was assumed to be $c/10$. The wave amplitude was 0.2 nT. From equation (4), the change in pitch will be proportional to the wave amplitude B, interaction time Δt, and the electron cyclotron frequency. The interaction time is the ratio of the spatial length X of the wave packet to the particle parallel speed $v_{||}$. Thus, the change in pitch angle is proportional to $BX/mv_{||}$. Assuming same chorus wave amplitude (0.2 nT), the 23 keV electron interactions of *Tsurutani et al.* [2009] can be compared with 1 MeV electron interactions. The amount of pitch angle scatter for relativistic ~ 1 MeV electrons then becomes less than 1°. This indicates that the relativistic electron scattering with whistler mode chorus waves, even if they are coherent, is minor in comparison.

4.1.1. L Shell Variations

Quasi-coherent EMIC waves have also been detected at other L values along the Cassini pass other than $L = 9$. Cassini crossed the $L = 10$ shell at ~0227 UT and $L = 8$ shell at ~0239 UT. The pitch angle scattering rates at these L shells using the measured values of the wave amplitude and other pertinent parameters were calculated and are displayed in Table 1. For $L = 6$ and 7, there were no waves found. Thus, for this example, the wave-particle interactions would all take place at very large L.

In order to have a comparison of pitch angle scattering at various L shells, we assume that relativistic electrons will cyclotron resonate with EMIC waves of frequency $\omega = 3$ rad/s and amplitude $B = 0.44$ nT at these L shells. Thirty second duration wave packets were also assumed. The magnetic field magnitude and the densities at various L shells and at different latitudes are calculated assuming a dipole field model of the Earth.

The resonant energies of the electrons shown in the Table are noted to increase with lower L shells, implying that proton cyclotron waves can pitch angle transport higher-energy (>1 MeV) electrons at lower L shells (assuming the wave frequency is constant).

4.1.2. Latitudinal Variations

Plasma densities and the magnetic field magnitude also vary with respect to latitude λ on a given field line (L shell). Assuming that the wave frequency and amplitude do not change as the wave propagates along B_0, the pitch angle scattering rates at various geomagnetic latitudes are calculated. The results for $L = 9$ field line are tabulated in Table 2. The pitch angle transport $\Delta\alpha$ at the magnetic equator is ~28° and decreases as one moves to higher latitudes. It is noted that above ~20° geomagnetic latitude the electron parallel speed must be greater than c (the speed of light) for resonance, so that is a cutoff for wave-particle interaction. Thus,

Table 2. Pitch Angle Scattering at Different Latitudes ($L = 9$)

λ (deg)	v_{ph} $\times 10^5$ (m/s)	Ω_e $\times 10^4$ (rad/s)	ω (rad/s)	$v_{\|\|}$ $\times 10^8$ (m/s)	γ	$E_{\|\|}$ (MeV)	Δt (ms)	$\Delta\alpha$ (deg)	D (s^{-1})	T (ms)
0	2.10	0.97	2.25	2.847	3.17	0.73	21.9	28	5.4	185
10	2.26	1.11	2.25	2.896	3.83	0.91	23.2	24	3.9	256
15	2.38	1.30	2.25	2.930	4.66	1.14	24.1	21	2.75	364
20	2.61	1.63	2.25	**3.065**	∞	∞	-	-	-	-

EMIC waves are only effective within ±20° geomagnetic latitudes. The angular and energy ranges were shown for illustration assuming a dipole magnetic field. The numbers will change for a dayside flattened field with minimum B pockets. The numbers will also change with L shell.

5. Discussion and Conclusions

Electromagnetic electron/proton cyclotron waves are excited in the magnetosphere during high solar wind dynamic pressure conditions. EMIC wave properties and their external causes have been previously reported by *Anderson and Hamilton* [1993], *Engebretson et al.* [2002], and *Usanova et al.* [2012]. The compression of preexisting ~10–100 keV electrons and protons induces a temperature anisotropy $T_\perp > T_\parallel$ for both particles, and hence, simultaneous EMIC and chorus waves occur.

EMIC waves are found to be large-amplitude, circular to elliptical polarizations with slightly oblique propagation relative to the ambient magnetic field. EMIC waves are coherent to quasi-coherent and are believed to be generated by anisotropic ~10–100 keV ions. EMIC waves should be responsible for the precipitation of the ~10–100 keV ions from the magnetosphere to the ionosphere/atmosphere causing a diffuse proton aurora [*Sakaguchi et al.*, 2008]. However, here we note that the waves can also anomalously cyclotron resonate with relativistic electrons and lead to the rapid precipitation of relativistic electrons as well [*Miyoshi et al.*, 2008; *Usanova et al.*, 2014].

Anomalous cyclotron resonant interaction calculations of EMIC waves with relativistic electrons show that for a measured EMIC wave packet detected at the equator at $L = 9$, the pitch angle transport of ~0.9 MeV electrons will be 27° in a 23 ms interaction. At the same time, the pitch angle scattering of relativistic electrons resulting from their resonant cyclotron interaction with observed chorus element can be at the most 1°. Thus, the loss rate of relativistic electrons resulting from their anomalous coherent cyclotron resonance interaction with an EMIC wave packet is much higher than that of chorus. It is interesting to note that pitch angle transport of relativistic electron by EMIC wave packets is much higher as compared to that reported for coherent chorus wave interaction with nonrelativistic electrons which is about 7° [*Lakhina et al.*, 2010; *Tsurutani et al.*, 2009]. Hence, it is anticipated that relativistic electron interaction with coherent chorus waves are unlikely to create relativistic microbursts. Calculations also show that cyclotron resonance between EMIC waves and relativistic electrons can only occur within 20° of the magnetic equator. Cyclotron resonance is not possible at large magnetic latitudes.

Relativistic electron cyclotron resonance with coherent EMIC waves (first shown here) will lead to a loss rate that is orders of magnitude higher than that for incoherent waves. This is because the individual particles are phase locked with the coherent signal for distances of many wavelengths and undergo large net pitch angle changes in a single wave packet-particle encounter. Hence, coherent waves are more efficient in scattering the particles from the magnetosphere.

Understanding the process of loss of relativistic electrons from the Earth's magnetosphere will help us unveil the radiation belt loss mechanisms which is a major topic of study in the present scenario. Apart from chorus, EMIC waves are long suggested to account for the rapid loss of radiation belt relativistic electrons via cyclotron resonance [*Thorne and Kennel*, 1971; *Horne and Thorne*, 1998; *Summers et al.*, 1998; *Albert*, 2003; *Summers and Thorne*, 2003; *Summers et al.*, 2007a, 2007b; *Thorne*, 2010]. This paper validates the idea and shows EMIC to be an efficient scatter mechanism for relativistic electrons as compared to chorus waves.

6. Final Comments

The outer zone, local noon EMIC waves reported here are consistent with a solar wind pressure pulse generation mechanism accelerating preexisting ~10–100 keV protons in $E_\perp$ with consequential instability generating the waves [*Olson and Lee*, 1983; *Anderson and Hamilton*, 1993; *Tsurutani et al.*, 2001; *Engebretson et al.*, 2002; *Usanova et al.*, 2012]. The waves shown in this paper lacked obvious rising tone structures. At this time we do not know if this is the "broadband EMIC" emission that is discussed by *Shoji and Omura* [2014]. The latter authors speculate that such features may be due to the rapid scattering of energetic protons into the loss cone, breaking up the coherent rising tones. Our calculations show that there should be ~23 ms structure in relativistic ~0.9 MeV electron precipitation due to the electron interaction with ~30 s duration coherent EMIC waves. However, because the EMIC wave packet durations are irregular, the precipitation pulses will be irregular as well. If we do the same calculation for ~30 keV parallel propagating protons, we get

interaction times of ~2–3 s. The relativistic electron temporal structure is probably not measurable due to the low flux levels. However, the proton structures might be measurable by satellites and rockets at the top of the ionosphere. The proton aurora itself may not show such time structure due to the nature of the excitation mechanism [*Immel et al.*, 2002; *Sakaguchi et al.*, 2008]. The same general feature is expected for ~10–100 keV electron microbursts. The interaction time scales between the energetic electrons and chorus subelements are ~3 ms [*Tsurutani et al.*, 2009, 2013b]. But again, the chorus subelement scale sizes are irregular and thus the microburst substructures will be as well.

Acknowledgments

B. Remya would like to thank Indian Institute of Geomagnetism, Navi Mumbai, India, for providing her with Nanabhoy Moos Postdoctoral Fellowship to carry out this research work. Portions of this research were performed at the Jet Propulsion Laboratory, California Institute of Technology under contract with NASA. G.S.L. thanks the National Academy of Sciences, India (NASI) for the support under the NASI-Senior Scientist Platinum Jubilee Fellowship. The solar wind and interplanetary magnetic field data are obtained from the OMNI website (http://omniweb.gsfc.nasa.gov/). One minute *AE* indices and 1 h *SYM-H* indices were obtained from the World Data Center for Geomagnetism, Kyoto, Japan (http://wdc.kugi.kyoto-u.ac.jp/). The integrated fluxes of electrons with energies $E > 2.0$ MeV are obtained from GOES-8 (http://www.ngdc.noaa.gov/stp/satellite/goes/dataaccess.html). The Cassini fluxgate magnetometer data are obtained from NASA Planetary Data System (http://ppi.pds.nasa.gov/).

Michael Balikhin thanks the reviewers for their assistance in evaluating this paper.

References

Albert, J. M. (2003), Evaluation of quasi-linear diffusion coefficients for EMIC waves in a multispecies plasma, *J. Geophys. Res.*, *108*(A6), 1249, doi:10.1029/2002JA009792.

Anderson, B. J., and D. C. Hamilton (1993), Electromagnetic ion cyclotron waves stimulated by modest magnetospheric compressions, *J. Geophys. Res.*, *98*(A7), 11,369–11,382, doi:10.1029/93JA00605.

Balogh, A., et al. (1999), The solar origin of corotating interaction regions and their formation in the inner heliosphere, *Space Sci. Rev.*, *89*, 141–178.

Belcher, J. W., and L. Davis Jr. (1971), Large-amplitude Alfvén waves in the interplanetary medium, 2, *J. Geophys. Res.*, *76*, 3534–3563.

Brice, N., and C. Lucas (1971), Influence of magnetospheric convection and polar wind on loss of electrons from the outer radiation belt, *J. Geophys. Res.*, *76*(4), 900–908, doi:10.1029/JA076i004p00900.

Cornwall, J. M. (1965), Cyclotron instabilities and electromagnetic emission in the ultra low frequency and very low frequency ranges, *J. Geophys. Res.*, *70*(1), 61–69, doi:10.1029/JZ070i001p00061.

Cornwall, J. M., and M. Schulz (1971), Electromagnetic ion-cyclotron instabilities in multicomponent magnetospheric plasmas, *J. Geophys. Res.*, *76*, 7791–7796, doi:10.1029/JA076i031p07791.

DeForest, S. E., and C. E. McIlwain (1971), Plasma clouds in the magnetosphere, *J. Geophys. Res.*, *76*, 3587–3611, doi:10.1029/JA076i016p03587.

Delport, B., A. B. Collier, J. Lichtenberger, C. J. Rodger, M. Parrot, M. A. Clilverd, and R. H. W. Friedel (2012), Simultaneous observation of chorus and hiss near the plasmapause, *J. Geophys. Res.*, *117*, A12218, doi:10.1029/2012JA017609.

Dungey, J. W. (1961), Interplanetary magnetic field and the auroral zones, *Phys. Rev. Lett.*, *6*, 47–48.

Engebretson, M. J., W. K. Peterson, J. L. Posch, M. R. Klatt, B. J. Anderson, C. T. Russell, H. J. Singer, R. L. Arnoldy, and H. Fukunishi (2002), Observations of two types of Pc 1-2 pulsations in the outer dayside magnetosphere, *J. Geophys. Res.*, *107*(A12), 1451, doi:10.1029/2001JA000198.

Erlandson, R. E., and A. J. Ukhorskiy (2001), Observations of electromagnetic ion cyclotron waves during geomagnetic storms: Wave occurrence and pitch angle scattering, *J. Geophys. Res.*, *106*(A3), 3883–3895, doi:10.1029/2000JA000083.

Fraser, B. J., and R. L. McPherron (1982), Pc 1-2 magnetic pulsation spectra and heavy ion effects at synchronous orbit: ATS 6 results, *J. Geophys. Res.*, *87*(A6), 4560–4566, doi:10.1029/JA087iA06p04560.

Gerald, C. F., and P. O. Wheatley (2004), *Applied Numerical Analysis*, 7th ed., Pearson Educ., Addison-Wesley Co., Boston, Mass.

Gonzalez, W. D., and F. S. Mozer (1974), A quantitative model for the potential resulting from reconnection with an arbitrary interplanetary magnetic field, *J. Geophys. Res.*, *79*, 4186–4194, doi:10.1029/JA079i028p04186.

Halford, A. J., B. J. Fraser, and S. K. Morley (2010), EMIC wave activity during geomagnetic storm and nonstorm periods: CRRES results, *J. Geophys. Res.*, *115*, A12248, doi:10.1029/2010JA015716.

Hajra, R., E. Echer, B. T. Tsurutani, and W. D. Gonzalez (2013), Solar cycle dependence of high-intensity long-duration continuous AE activity (HILDCAA) events, relativistic electron predictors, *J. Geophys. Res. Space Physics*, *118*, 5626–5638, doi:10.1002/jgra.50530.

Hajra, R., B. T. Tsurutani, E. Echer, and W. D. Gonzalez (2014), Relativistic electron acceleration during high-intensity long-duration continuous AE activity (HILDCAA) events: Solar cycle phase dependences, *Geophys. Res. Lett.*, *41*, 1876–1881, doi:10.1002/2014GL059383.

Hajra, R., B. T. Tsurutani, E. Echer, W. D. Gonzalez, and O. Santolik (2015), Relativistic (E > 0,6, 2.0 and > 4.0 MeV) electron acceleration at geosynchronous orbit during high-intensity long-duration continuous AE activity (HILDCAA) events, *Astrophys. J.*, *799*(1), 39, doi:10.1088/0004-637X/799/1/39.

Hayakawa, M., Y. Tanaka, S. S. Sazhin, T. Okada, and K. Kurita (1986), Characteristics of dawnside midlatitude VLF emissions associated with substorms as deduced from the two-stationed direction finding measurement, *Planet. Space Sci.*, *34*, 225–243.

Horne, R. B., and R. M. Thorne (1998), Potential waves for relativistic electron scattering and stochastic acceleration during magnetic storms, *Geophys. Res. Lett.*, *25*, 3011–3014, doi:10.1029/98GL01002.

Immel, J., S. B. Mende, H. U. Frey, L. M. Peticolas, C. W. Carlson, J.-C. Geŕard, B. Hubert, S. A. Fuselier, and J. L. Burch (2002), Precipitation of auroral protons in detached arcs, *Geophys. Res. Lett.*, *29*(11), 1519, doi:10.1029/2001GL013847.

Inan, U. S., T. F. Bell, and R. A. Helliwell (1978), Nonlinear pitch angle scattering of energetic electrons by coherent VLF waves in the magnetosphere, *J. Geophys. Res.*, *83*(A7), 3235–3253, doi:10.1029/JA083iA07p03235.

Jentsch, V. (1976), Electron precipitation in the morning sector of the auroral zone, *J. Geophys. Res.*, *81*(1), 135–146, doi:10.1029/JA081i001p00135.

Kennel, C. F., and H. E. Petschek (1966), Limit on stably trapped particle fluxes, *J. Geophy. Res.*, *71*, 1–28.

Kennel, C. F., J. P. Edmiston, and T. Hada (1985), A quarter century of collisionless shock research, in *Collisionless Shocks in the Heliosphere: A Tutorial Review*, edited by R. G. Stone and B. T. Tsurutani, pp. 1–36, AGU, Washington, D. C., doi:10.1029/GM034p0001.

Koons, H. C., and J. L. Roeder (1990), A survey of equatorial magnetospheric wave activity between 5 and 8 R_E, *Planet. Space Sci.*, *38*, 1335–1341, doi:10.1016/0032-0633(90)90136-E.

Lakhina, G. S., B. T. Tsurutani, O. P. Verkhoglyadova, and J. S. Pickett (2010), Pitch angle transport of electrons due to cyclotron interactions with the coherent chorus subelements, *J. Geophys. Res.*, *115*, A00F15, doi:10.1029/2009JA014885.

Lauben, D. S., U. S. Inan, T. F. Bell, and D. A. Gurnett (2002), Source characteristics of ELF/VLF chorus, *J. Geophys. Res.*, *107*(A12), 1429, doi:10.1029/2000JA003019.

LeDocq, M. J., D. A. Gurnett, and G. B. Hospodarsky (1998), Chorus source locations from VLF Poynting flux measurements with the Polar spacecraft, *Geophys. Res. Lett.*, *25*, 4063–4066, doi:10.1029/1998GL900071.

Li, W., et al. (2013), An unusual enhancement of low-frequency plasmaspheric hiss in the outer plasmasphere associated with substorm-injected electrons, *Geophys. Res. Lett.*, *40*, 3798–3803, doi:10.1002/grl.50787.

Matsuda, S., Y. Kasahara, and Y. Goto (2014), Electromagnetic ion cyclotron waves suggesting minor ion existence in the inner magnetosphere observed by the Akebono satellite, *J. Geophys. Res. Space Physics*, *119*, 4348–4357, doi:10.1002/2013JA019370.

Meredith, N. P., R. B. Horne, and R. R. Anderson (2001), Substorm dependence of chorus amplitudes: Implications for the acceleration of electrons to relativistic energies, *J. Geophys. Res.*, *106*, 13,165–13,178.

Meredith, N. P., R. M. Thorne, R. B. Horne, D. Summers, B. J. Fraser, and R. R. Anderson (2003), Statistical analysis of relativistic electron energies for cyclotron resonance with EMIC waves observed on CRRES, *J. Geophys. Res.*, *108*(A6), 1250, doi:10.1029/2002JA009700.

Meredith, N. P., R. B. Horne, A. Sicard-Piet, D. Boscher, K. H. Yearby, W. Li, and R. M. Thorne (2012), Global model of lower band and upper band chorus from multiple satellite observations, *J. Geophys. Res.*, *117*, A10225, doi:10.1029/2012JA017978.

Miyoshi, Y., K. Sakaguchi, K. Shiokawa, D. Evans, J. Albert, M. Connors, and V. Jordanova (2008), Precipitation of radiation belt electrons by EMIC waves, observed from ground and space, *Geophys. Res. Lett.*, *35*, L23101, doi:10.1029/2008GL035727.

Olson, J. V., and L. C. Lee (1983), Pc1 wave generation by sudden impulses, *Planet. Space Sci.*, *31*(3), 295–297, doi:10.1016/0032-0633(83)90079-X.

Omura, Y., Y. Katoh, and D. Summers (2008), Theory and simulation of the generation of whistler mode chorus, *J. Geophys. Res.*, *113*, A04223, doi:10.1029/2007JA012622.

Papadopoulos, K. (1985), Microinstabilities and anomalous transport, in *Collisionless Shocks in the Heliosphere: A Tutorial Review*, edited by R. G. Stone and B. T. Tsurutani, 59 pp., AGU, Washington, D. C., doi:10.1029/GM034p0059.

Pizzo, V. J. (1985), Interplanetary shocks on the large scale: A retrospective on the last decade's theoretical effects, in *Collisionless Shocks in the Heliosphere: Reviews of Current Research, Geophys. Monogr. Ser.*, vol. 35, edited by B. T. Tsurutani and R. G. Stone, 51 pp., AGU, Washington, D. C., doi:10.1029/GM035p0051.

Remya, B., B. T. Tsurutani, R. V. Reddy, G. S. Lakhina, B. J. Falkowski, E. Echer, and K.-H. Glassmeier (2014), Large-amplitude, circularly polarized, compressive, obliquely propagating electromagnetic proton cyclotron waves throughout the Earth's magnetosheath: Low plasma β conditions, *Astrophys. J.*, *793*, 6, doi:10.1088/0004-637X/793/1/6.

Ronnmark, K. (1982), WHAMP: Waves in homogeneous anisotropic multicomponent plasma, *Kiruna Geophys. Inst. Rep. 179*, Kiruna Geophys. Inst., Kiruna, Sweden.

Sakaguchi, K., K. Shiokawa, Y. Miyoshi, Y. Otsuka, T. Ogawa, K. Asamura, and M. Connors (2008), Simultaneous appearance of isolated auroral arcs and Pc 1 geomagnetic pulsations at subauroral latitudes, *J. Geophys. Res.*, *113*, A05201, doi:10.1029/2007JA012888.

Shoji, M., and Y. Omura (2014), Spectrum characteristics of electromagnetic ion cyclotron triggered emissions and associated energetic proton dynamics, *J. Geophys. Res. Space Physics*, *119*, 3480–3489, doi:10.1002/2013JA019695.

Smith, E. J., and B. T. Tsurutani (1976), Magnetosheath lion roars, *J. Geophys. Res.*, *81*(13), 2261–2266, doi:10.1029/JA081i013p02261.

Smith, E. J., and J. H. Wolfe (1976), Observations of interaction regions and corotating shocks between one and five AU: Pioneers 10 and 11, *Geophys. Res. Lett.*, *3*, 137–140, doi:10.1029/GL003i003p00137.

Sonnerup, B. U. O., and L. J. Cahill Jr. (1967), Magnetopause structure and attitude from Explorer 12 observations, *J. Geophys. Res.*, *72*, 171–183, doi:10.1029/JZ072i001p00171.

Southwood, D. J., et al. (2001), Magnetometer measurements from the Cassini Earth swing-by, *J. Geophys. Res.*, *106*, 30,109–30,128.

Summers, D., and R. M. Thorne (2003), Relativistic electron pitch-angle scattering by electromagnetic ion cyclotron waves during geomagnetic storms, *J. Geophys. Res.*, *108*(A4), 1143, doi:10.1029/2002JA009489.

Summers, D., B. Ni, and N. P. Meredith (2007a), Timescales for radiation belt electron acceleration and loss due to resonant waveparticle interactions: 1. Theory, *J. Geophys. Res.*, *112*, A04206, doi:10.1029/2006JA011801.

Summers, D., B. Ni, and N. P. Meredith (2007b), Timescale for radiation belt electron acceleration and loss due to resonant wave-particle interactions: 2. Evaluation for VLF chorus, ELF hiss, and electromagnetic ion cyclotron waves, *J. Geophys. Res.*, *112*, A04207, doi:10.1029/2006JA011993.

Summers, D., R. M. Thorne, and F. Xiao (1998), Relativistic theory of wave-particle resonant diffusion with application to electron acceleration in the magnetosphere, *J. Geophys. Res.*, *103*(A9), 20,487–20,500, doi:10.1029/98JA01740.

Thorne, R. M. (2010), Radiation belt dynamics: The importance of wave-particle interactions, *Geophys. Res. Lett.*, *37*, L22107, doi:10.1029/2010GL044990.

Thorne, R. M., and C. F. Kennel (1971), Relativistic electron precipitation during magnetic storm main phase, *J. Geophys. Res.*, *76*(19), 4446–4453, doi:10.1029/JA076i019p04446.

Thorne, R. M., E. J. Smith, K. J. Fiske, and S. R. Church (1974), Intensity variation of ELF hiss and chorus during isolated substorms, *Geophys. Res. Lett.*, *1*, 193–196, doi:10.1029/GL001i005p00193.

Thorne, R. M., S. R. Church, W. J. Malloy, and B. T. Tsurutani (1977), The local time variation of ELF emissions during periods of substorm activity, *J. Geophys. Res.*, *82*(10), 1585–1590, doi:10.1029/JA082i010p01585.

Thorne, R. M., T. P. O'Brien, Y. Y. Shprits, D. Summers, and R. B. Horne (2005), Timescale for MeV electron microburst loss during geomagnetic storms, *J. Geophys. Res.*, *110*, A09202, doi:10.1029/2004JA010882.

Thorne, R. M., et al. (2013), Rapid local acceleration of relativistic radiation-belt electrons by magnetospheric chorus, *Nature*, *504*, 411–414.

Tsurutani, B. T., and W. D. Gonzalez (1987), The cause of high-intensity long-duration continuous AE activity (HILDCAAs): Interplanetary Alfvn wave trains, *Planet. Space Sci.*, *35*, 405–412.

Tsurutani, B. T., and G. S. Lakhina (1997), Some basic concepts of wave-particle interactions in collisionless plasmas, *Rev. Geophys.*, *35*(4), 491–501, doi:10.1029/97RG02200.

Tsurutani, B. T., and E. J. Smith (1974), Postmidnight chorus: A substorm phenomenon, *J. Geophys. Res.*, *79*(1), 118–127, doi:10.1029/JA079i001p00118.

Tsurutani, B. T., and E. J. Smith (1977), Two types of magnetospheric ELF chorus and their substorm dependences, *J. Geophys. Res.*, *82*(32), 5112–5128, doi:10.1029/JA082i032p05112.

Tsurutani, B. T., E. J. Smith, and R. M. Thorne (1975), Electromagnetic hiss and relativistic electron losses in the inner zone, *J. Geophys. Res.*, *80*(4), 600–607, doi:10.1029/JA080i004p00600.

Tsurutani, B. T., E. J. Smith, H. I. West Jr., and R. M. Buck (1979), Chorus, energetic electrons and magnetospheric substorms, in *Wave Instabilities in Space Plasmas*, vol. 55, edited by P. Palmadesso and K. Papadopoulos, pp. 55–62, D. Reidel, Dordrecht, Netherlands.

Tsurutani, B. T., W. D. Gonzalez, F. Tang, S. I. Akasofu, and E. J. Smith (1988), Origin of interplanetary southward magnetic fields responsible for major magnetic storms near solar maximum (1978–1979), *J. Geophys. Res.*, *93*(A8), 8519–8531, doi:10.1029/JA093iA08p08519.

Tsurutani, B. T., W. D. Gonzalez, A. L. C. Gonzalez, F. Tang, J. K. Arballo, and M. Okada (1995), Interplanetary origin of geomagnetic activity in the declining phase of the solar cycle, *J. Geophys. Res.*, *100*, 21,717–21,733, doi:10.1029/95JA01476.

Tsurutani, B. T., X.-Y. Zhou, V. M. Vasyliunas, G. Haerendel, J. K. Arballo, and G. S. Lakhina (2001), Interplanetary shocks, magnetopause boundary layers and dayside auroras: The importance of a very small magnetospheric region, *Surv. Geophys.*, *22*(2), 101–130.

Tsurutani, B. T., et al. (2006), Corotating solar wind streams and recurrent geomagnetic activity: A review, *J. Geophys. Res.*, *111*, A07S01, doi:10.1029/2005JA011273.
Tsurutani, B. T., O. P. Verkhoglyadova, G. S. Lakhina, and S. Yagitani (2009), Properties of dayside outer zone chorus during HILDCAA events: Loss of energetic electrons, *J. Geophys. Res.*, *114*, A03207, doi:10.1029/2008JA013353.
Tsurutani, B. T., G. S. Lakhina, O. P. Verkhoglyadova, W. D. Gonzalez, E. Echer, and F. L. Guarnieri (2011a), A review of interplanetary discontinuities and their geomagnetic effects, *J. Atmos. Sol. Terr. Phys.*, *73*(1), 5–19, doi:10.1016/j.jastp.2010.04.001.
Tsurutani, B. T., B. J. Falkowski, O. P. Verkhoglyadova, J. S. Pickett, O. Santolík, and G. S. Lakhina (2011b), Quasi-coherent chorus properties: 1. Implications for wave-particle interactions, *J. Geophys. Res.*, *116*, A09210, doi:10.1029/2010JA016237.
Tsurutani, B. T., E. Echer, I. Richter, C. Koenders, and K.-H. Glassmeier (2013a), SLAMS at comet 19P/Borrelly: DS1 observations, *Planet. Space Sci.*, *75*, 17–27.
Tsurutani, B. T., G. S. Lakhina, and O. P. Verkhoglyadova (2013b), Energetic electron (>10 keV) microburst precipitation, ~5–15 s X-ray pulsations, chorus, and wave-particle interactions: A review, *J. Geophys. Res. Space Physics*, *118*, 2296–2312, doi:10.1002/jgra.50264.
Turner, D. L., et al. (2014), On the cause and extent of outer radiation belt losses during the 30 September 2012 dropout event, *J. Geophys. Res. Space Physics*, *119*, 1530–1540, doi:10.1002/2013JA019446.
Usanova, M. E., I. R. Mann, J. Bortnik, L. Shao, and V. Angelopoulos (2012), THEMIS observations of electromagnetic ion cyclotron wave occurrence: Dependence on AE, SYMH, and solar wind dynamic pressure, *J. Geophys. Res. Space Physics*, *117*, A10218, doi:10.1029/2012JA018049.
Usanova, M. E., et al. (2014), Effect of EMIC waves on relativistic and ultrarelativistic electron populations: Groundbased and Van Allen Probes observations, *Geophys. Res. Lett.*, *41*, 1375–1381, doi:10.1002/2013GL059024.
Vasyliunas, V. M. (1975), An overview of magnetospheric dynamics, in *Magnetospheric Particles and Fields*, edited by B. M. McCormac, 99 pp., D. Reidel, Hingham, Mass.
Verkhoglyadova, O. P., B. T. Tsurutani, Y. Omura, and S. Yagitani (2009), Properties of nonlinear rising tone chorus emissions observed by GEOTAIL on April 29, 1993, *Earth Planets Space*, *61*(5), 625–628, doi:10.1186/BF03352937.
Verkhoglyadova, O. P., B. T. Tsurutani, and G. S. Lakhina (2010), Properties of obliquely propagating chorus, *J. Geophys. Res.*, *115*, A00F19, doi:10.1029/2009JA014809.

6. Erratum

In the originally published version of this article, there were several small errors in the text and in Figures 7 and 8. The text and figures have since been corrected, and this version may be considered the authoritative version of record.